International Journal of Materials Research 103 (2012) 476-482

Bainite: Fragmentation of crystallographically homogeneous domains

Junhak Pak[a], Dong Woo Suh[a] and H. K. D. H. Bhadeshia[a,b]

[a]Graduate Institute of Ferrous Technology,
Pohang University of Science and Technology, Pohang, Republic of Korea

[b]Materials Science and Metallurgy,
University of Cambridge, Pembroke Street, Cambridge, U.K.

It becomes possible in appropriate circumstances for similarly oriented plates of bainite or martensite to merge and form coarse crystallographically homogeneous domains whose presence leads to a deterioration in mechanical properties. A method is presented here for breaking up such domains, by introducing very small scale chemical composition variations in the austenite prior to its transformation.

Keywords: Bainite; Crystallographic grain size; Segregation; Intercritical annealing; Refinement

1 Introduction

The advent of orientation imaging has led to discoveries in which the relationship between the scale of structure and properties has been generalised to include 'crystallographic grain size', implying the size over which cleavage cracks are not significantly deviated. This size may include clusters of grains as observed using ordinary microscopy where individual crystals are distinguished by etching to reveal boundaries [1–5]. The subject has been reviewed by Gourgues–Lorenzon [6].

The mechanism by which the coarse regions develop is usually to do with the presence of strong texture induced by deformation or phase transformation. In the case where austenite transforms into bainite or martensite, groups of plates can form with the same orientation in space, leading to the formation of packets across which there is little misorientation [7, 8]. There is also another subtle process in which thin platelets of martensite or bainite which grow on parallel habit planes and hence are identically oriented, merge during prolonged growth to form coarse blocks [9] which also lead to a deterioration in toughness. This leads to a markedly bimodal distribution of plate thicknesses, with the fine plates being about 0.2 μm thick and the larger plates many micrometres thick. The key requirements for coalescence to occur have been listed as follows [9]:

(i) there must be sufficient driving force to sustain the larger strain energy associated with thicker plates;

(ii) there should be nothing to stifle the growth of individual platelets since coalescence evolves gradually as the platelets merge.

There has been little work in general, on how to disrupt the formation of coarse crystallographic domains, and certainly none on the prevention of the plate coalescence process just described. It is the second of the conditions listed above that we hoped to exploit in order to develop a new method to hinder coalescence. Fine compositional perturbations are introduced into the austenite prior to its transformation, so as to prevent the merging of plates. As will be seen later, this has been achieved by heat–treatment in a two–phase field prior to full austenitisation and subsequent transformation. Although such a technique may not be cost–effective in general, it can in principle be implemented during multipass welding where the deposition of a new layer induces the heat treatment of the underlying material.

2 Experimental technique

The alloy listed in Table 1 was selected because of its propensity to form coalesced bainite [10, 11]. It was supplied by ESAB AB (Sweden) and machined into cylindrical dilatometric samples 3 mm in diameter and 10 mm in length. The machined samples were then sealed in quartz capsules under vacuum and homogenised for 2 days at 1300 °C.

A push-rod BAHR DIL805 high-speed dilatometer with radio frequency induction heating was used. The sample temperature is recorded by a thermocouple welded to its surface. X–ray diffractometry was used to identify the phases in the specimen. Metallography was conducted on the dilatometric specimens using optical microscopy and field emission gun scanning electron microscopy. For the purposes of electron backscattered diffraction, the final stages of sample preparation involved delicate polishing using colloidal silica. Transmission electron microscopy and its scanning variant were used for energy dispersive spectrometry on specimens detached using the focused ion beam technique.

3 Method

When a steel is annealed within the two–phase austenite (γ) and ferrite (α) field, austenite stabilising substitutional solutes such as manganese and nickel will tend to partition preferentially into γ. The tendency for such redistribution is defined by the equilibrium phase diagram. If a fully martensitic sample is annealed in this way, then small regions of solute–enriched austenite regions will form between the plates. With prolonged annealing, the composition and phase fractions of austenite and ferrite will reach equilibrium. A subsequent, short heat treatment in the single γ phase field can be designed so that the ferrite is eliminated but the non–uniform distribution of solute remains on a fine scale consistent with the original films of austenite generated at the intercritical annealing treatment.

The process is illustrated schematically in Fig. 1; chemically heterogeneous austenite is first created by intercritical annealing, to be followed by transformation into bainite. The regions rich in austenite are slow to transform and hence disrupt the growth of bainite originating from the solute–depleted austenite, thereby preventing coalescence of parallel plates.

4 Design of heat treatment

Calculations were carried out on the equilibrium phase fractions of austenite and ferrite in the steel listed in Table 1 as a function of temperature, using *Thermo-Calc* version S, as illustrated in Fig. 2; the plot deals with only austenite and ferrite because cementite is not a stable phase above 576 °C. As is evident, the extent to which the partitioning of solutes occurs increases

as the temperature is reduced, consistent also with the decrease in the equilibrium fraction of austenite. Hence, the intercritical annealing temperature was chosen as 580 °C (step b in Fig. 1).

The program *DICTRA* version 25 was used to assess the time required to achieve sufficient partitioning during intercritical annealing. Two simulations were conducted, the first where the austenite initially has the chemical composition of the alloy, i.e., it originates from the austenite that is retained when the steel is quenched to martensite. The second represents approximately the case where the calculation assumes local equilibrium at the interface between austenite and ferrite at the annealing temperature.

The kinetics of the partitioning of solutes through successive heat treatments was simulated using *DICTRA* version 25 considering only carbon, manganese and nickel as the diffusing species; the latter two were selected because they are present in significant concentrations. The calculations assumed as the starting state, the existence of a thin layer (0.01 μm) of austenite of the appropriate chemical compositions, attached to a 0.1 μm layer of ferrite. The volume fraction of austenite at the beginning is therefore less than equilibrium fraction at the chosen intercritical annealing temperature of 590 °C for the purposes of simulation. Notice that this is 10 °C greater than the 580 °C used in the experiments because a specific numerical issue with *DICTRA* which meant that the amount of nickel had to be adjusted slightly in order to avoid numerical instability for the 580 °C calculation [12]. It turns out that there is not much of a difference in the *DICTRA* output for the accurate calculation for 590 °C and approximate analysis for the 580 °C case, as illustrated in Fig. 3.

The next stage of the heat treatment is to fully austenitise the chemically–heterogeneous structure produced during intercritical annealing, in such a way that the heterogeneity is essentially preserved. The measured $Ac3$ temperature of the alloy at a heating rate of $50\,\mathrm{K\,s^{-1}}$ was found to be 742 ± 0.5 °C; the heating rate has to be high in order to avoid the substantial diffusion of substitutional solutes during heating. The austenitisation condition was set as 780 °C for 10 min because *DICTRA* simulation indicated that although diffusion is inevitable, the solute rich regions persist, as illustrated in Fig. 4. The simulation was conducted assuming an region of austenite enriched by intercritical annealing to a thickness of 8 nm and composition 5.8Mn–16.2Ni wt.%; the corresponding composition of ferrite was set at 1.1Mn–5.0Ni wt.%, consistent with the profile presented in Fig. 3; the approximation here is that any gradient within the 8 nm thick austenite is

neglected at the point where the simulation begins. There are small variations in the carbon concentration as a function of distance, but this is not because of a lack of atomic mobility, but rather that the chemical potential of carbon is homogenised in the presence of variations in the manganese and nickel concentrations.

5 Dilatometry

Using the information from the simulations, three different heat treatments were conducted in a dilatometer (Fig. 5). Two of these are from homogeneous austenite to obtain martensite or bainite, and the third to obtain bainite from heterogeneous austenite; the latter is for convenience, designated $\alpha_{\rm b}^{\rm h}$ in all subsequent discussion. The results are shown in Fig. 6, which reveal that some martensite was also obtained after the isothermal heat treatment to generate $\alpha_{\rm b}$ and $\alpha_{\rm b}^{\rm h}$.

The strain change due to austenite formation during intercritical annealing at 580 °C was found to be 0.0004, which compares with the strain of 0.0056 for full austenitisation at that temperature as judged from the first heat–treatment illustrated in Fig. 6. Thus, the fraction of austenite formed during annealing is estimated to be 0.07, although the total may be greater if the sample contained retained austenite prior to heating to 580 °C.

It is interesting that the amount of bainite obtained isothermally is greater in the homogeneous when compared with the heterogeneous austenite, Fig. 7a; this is consistent with previous observations and is a consequence of the fact that nucleation is generally confined to solute–depleted regions in a segregated steel [13, 14]. As a consequence, the amount of martensite is greater in the heterogeneous steel, Fig. 7b. It should be noted that X–ray diffraction failed to reveal any retained austenite in the heterogeneous sample in spite of the high solute concentration in localised regions, probably because of the low carbon concentration of the steel.

6 Characterisation

The microstructures are illustrated in Figs. 8 and 9 where an attempt has been made to distinguish between bainite and martensite purely on morphological basis. The heterogeneous sample was subjected to transmission

electron microscopy in order to establish the presence of substitutional–solute rich regions. Figure 10 is a region extracted using focused ion beam machining from bainite identified using scanning electron microscopy, in the heterogeneous sample. The circled area was then subjected to microanalysis traversing several boundaries. It is clear from Figs. 11 and 12 that the expected enrichment in manganese and nickel concentrations is indeed present.

The agreement between the microanalysis and the calculations using *DICTRA* can be considered to be reasonable given that the spatial resolution will be about the thickness of the foil (not measured, but likely to be around 50 nm), and it is not clear whether the scan direction is normal to the boundary concerned. The experiments establish clearly that the intercritical annealing and short austenitisation treatment succeeded in creating the postulated segregation of substitutional solutes. Some additional scan are shown in Fig. 13 to show that the enriched regions can be variable, probably because the dimensions of austenite regions formed during intercritical annealing are not likely to be uniform.

Image quality (IQ) mapping and inverse pole figures were determined on the bainite formed in homogeneous and heterogeneous austenite, as shown in Fig. 14. It is clear that the visualised boundaries in quality images are much denser in the bainite from the heterogeneous austenite. Furthermore, the crystallographic grain size is clearly finer with $\alpha_{\mathrm{b}}^{\mathrm{h}}$, so that the complex heat treatment has succeeded in fragmenting the structure from a crystal orientation point of view.

7 Conclusions

It is found that the introduction of chemical heterogeneities can break up the development of microstructure during the bainite transformation, thus resulting in a significantly refined crystallographic grain size.

Whereas this was achieved in the present work by introducing segregated regions using heat–treatment, it is possible that solidification–induced segregation, which is inevitably present in commercial steels, could in principle be exploited in the manner described in the paper, although other consequences of such segregation would have to be borne in mind during the investigation of this possibility.

We acknowledge Professor Nack Joon Kim for the provision of laboratory facilities at GIFT, and support from POSCO through the Steel Innovation Programme. The authors are also grateful for support from the World Class University Programme of the National Research Foundation of Korea, Ministry of Education, Science and Technology, project number R32–2008–000–10147–0. We are also grateful to Kim Dong Hwi for discussion and help with the transmission electron microscopy.

References

[1] A. F. Gourgues, H. M. Flower, T. C. Lindley, Materials Science and Technology 16 (2000) 26.

[2] A. Lambert-Perlade, A. F. Gourgues, A. Pineau, Acta Materialia 52 (2004) 2337.

[3] D. Bhattacharjee, J. F. Knott, C. L. Davis, Metallurgical & Materials Transactions A 35 (2004) 121.

[4] Y. M. Kim, S. Y. Shin, H. Lee, B. Wang, S. Lee, N. J. Kim, Metallurgical & Materials Transactions A 38 (2007) 1731.

[5] P. Yan, O. E. Güngör, P. Thibaux, H. K. D. H. Bhadeshia, Advanced Materials Research 89-91 (2010) 651.

[6] A. F. Gourgues-Lorenzon, International Materials Reviews 52 (2007) 65.

[7] J. P. Naylor, P. R. Krahe, Metallurgical Transactions 5 (1974) 1699.

[8] T. Maki, K. Tsuzaki, I. Tamura, Trans. Iron Steel Institute of Japan 20 (1980) 207.

[9] L. C. Chang, H. K. D. H. Bhadeshia, Materials Science and Technology 12 (1996) 233.

[10] E. Keehan, L. Karlsson, H.-O. Andrén, H. K. D. H. Bhadeshia, Welding Journal, Research Supplement 85 (2006) 200.

[11] E. Keehan, L. Karlsson, H.-O. Andrén, L.-E. Svensson, Welding Journal, Research Supplement 85 (2006) 211s.

[12] J. Bratberg, Private communication from DICTRA staff, 2011.

[13] S. A. Khan, H. K. D. H. Bhadeshia, Metallurgical Transactions A 21A (1990) 859.

[14] H. K. D. H. Bhadeshia, Bainite in Steels, 2nd edition, Institute of Materials, London, 2001.

Professor H. K. D. H. Bhadeshia

Materials Science and Metallurgy

University of Cambridge, Pembroke Street, Cambridge CB2 3QZ, U. K.

Tel +441223 334300 Fax +441223 334567

hkdb@cam.ac.uk

Table 1: Chemical composition of the alloy (wt.%) (Fe bal.)

C	Si	Mn	Cr	Ni	Mo
0.03	0.23	2.05	0.43	7.1	0.63

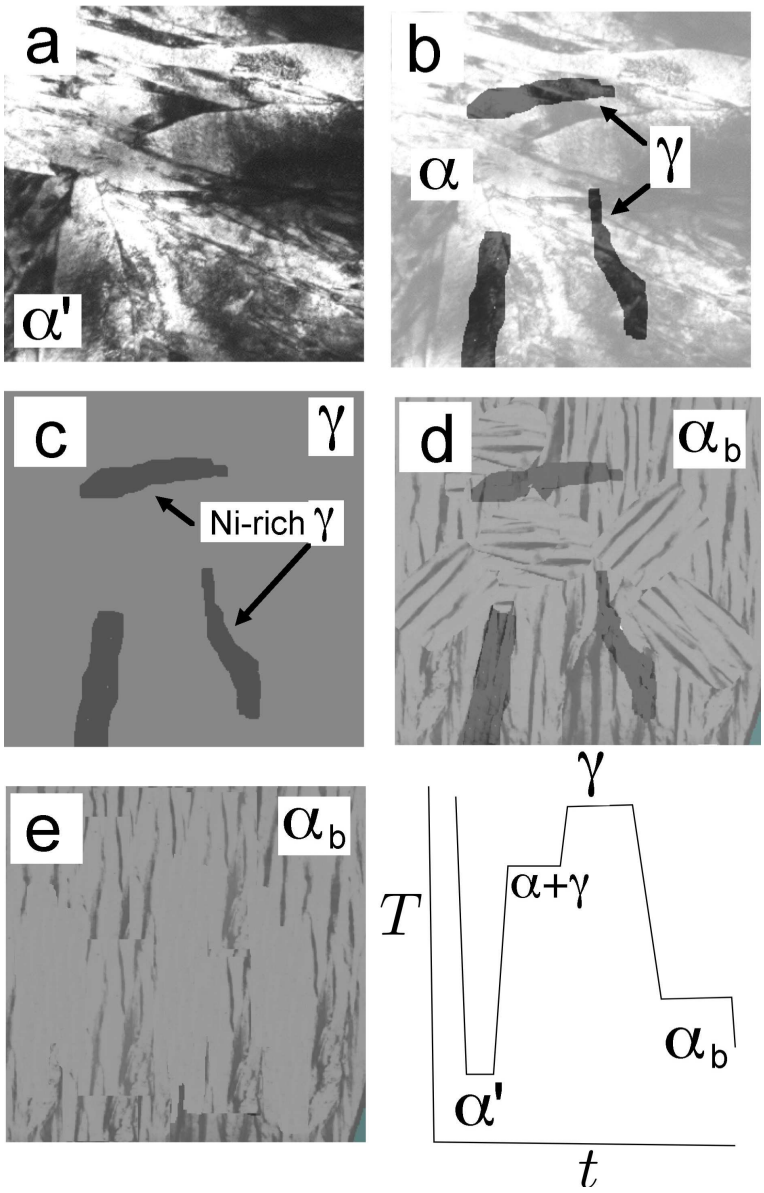

Figure 1: **Schematic** illustration of the method used to reduce the crystallographic grain size, beginning with (a) α' martensite; (b) intercritical annealing to produce small regions of enriched–austenite γ and α tempered martensite; (c) short treatment to eliminate α but leave the austenite compositionally modulated; (d) isothermal transformation of compositionally modulated γ to many orientations of α_b bainite; (e) bainite from homogeneous austenite, with a bimodal distribution consisting of coalesced and fine plates.

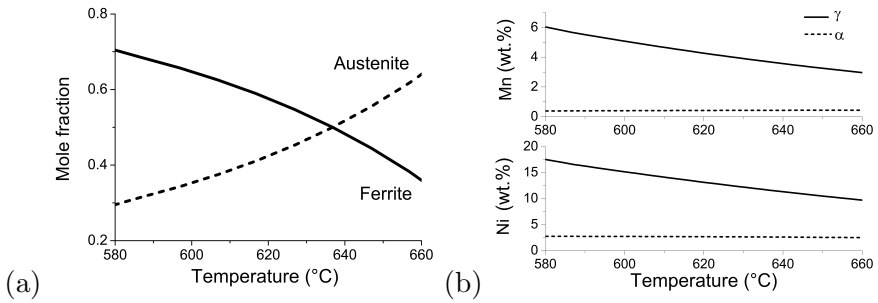

Figure 2: (a) Equilibrium fractions of austenite and ferrite as a function of the temperature. (b) Equilibrium chemical compositions of stable phases.

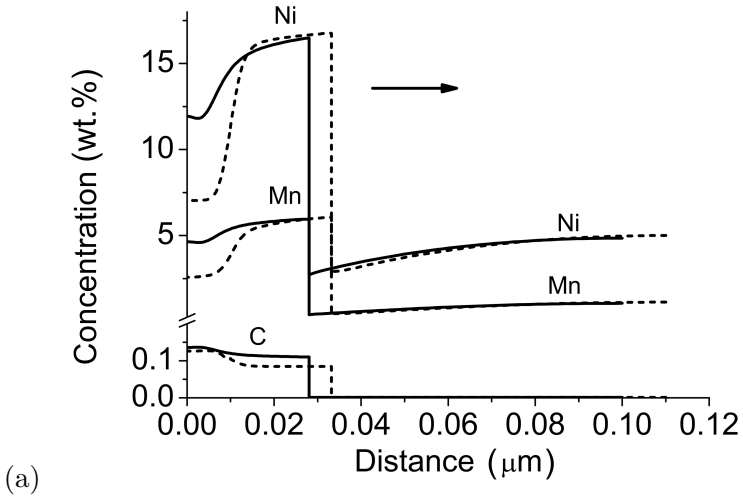

(a)

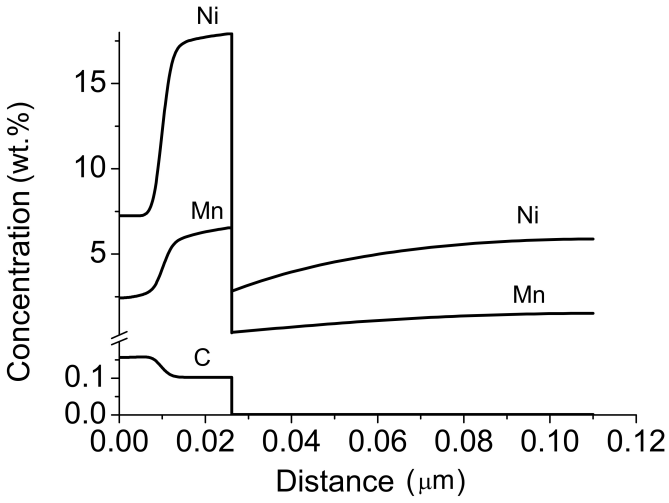

(b)

Figure 3: *DICTRA* simulations of solute partitioning during austenite growth over a period of 5 h. (a) 590 °C with the dashed line for austenite with a starting composition identical to that of the alloy, and the continuous line assuming that the austenite formed at 590 °C and hence has the equilibrium composition for that temperature. The arrow indicates the growth direction of the austenite. (b) 580 °C assuming that the starting austenite has the average composition of the alloy.

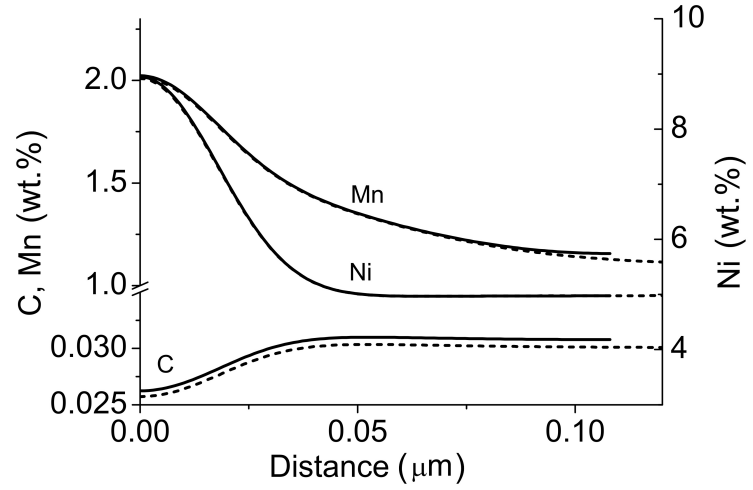

Figure 4: Simulation of the spread of alloying elements during austenitisation at 780 °C for 10 minutes. Solid lines and dotted lines correspond to the cases where the far–field distance over which diffusion is allowed was set at 0.108 and 1.008 μm, respectively.

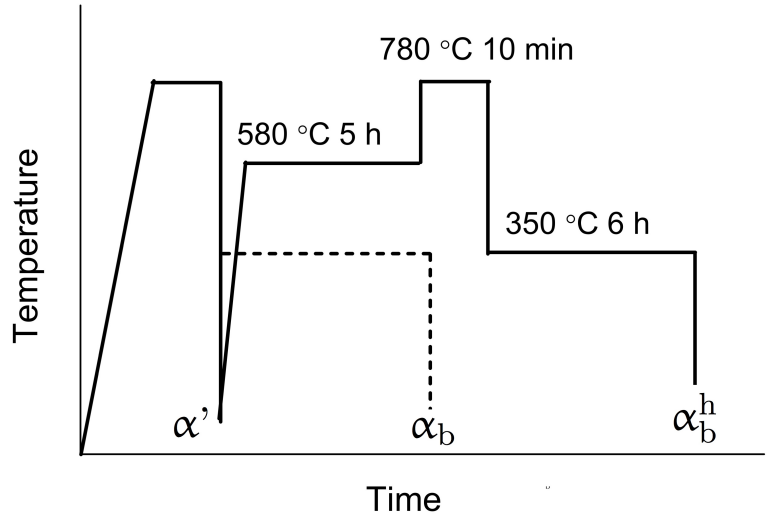

Figure 5: Illustration of the heat–treatments used to generate three different microstructures.

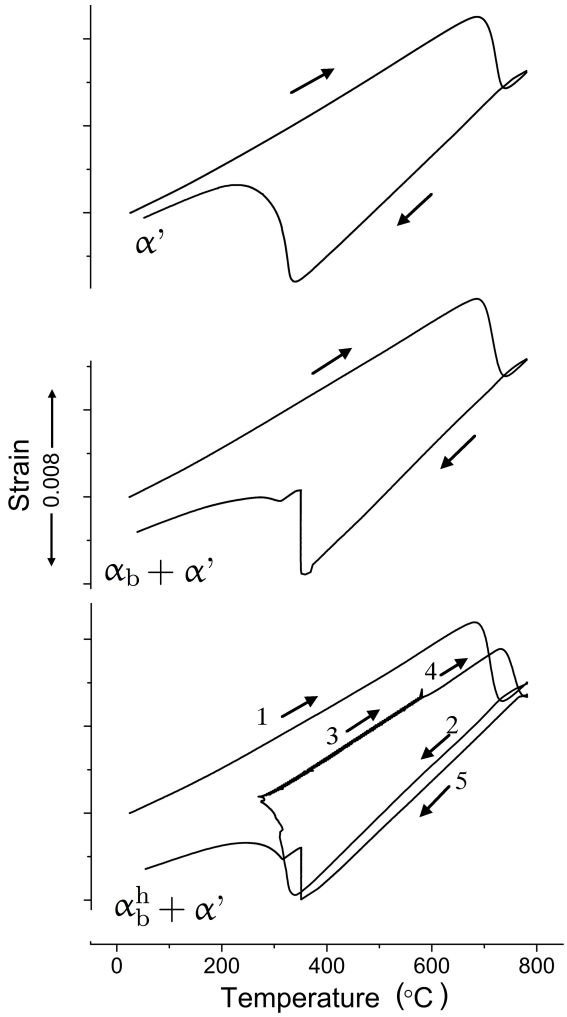

Figure 6: Dilatometer curves showing three different heat treatments

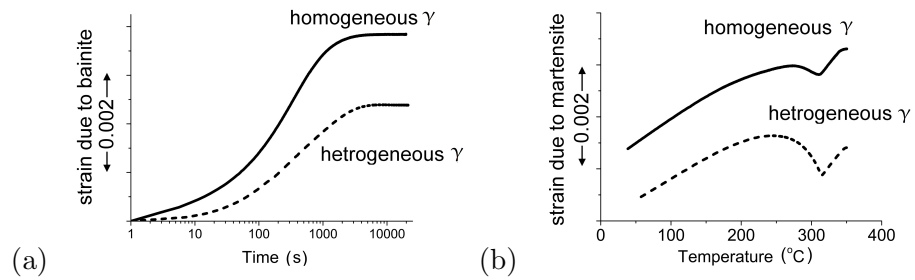

Figure 7: Dilatometric data for the (a) isothermal bainite transformation and (b) the martensite transformation which follows the formation of bainite.

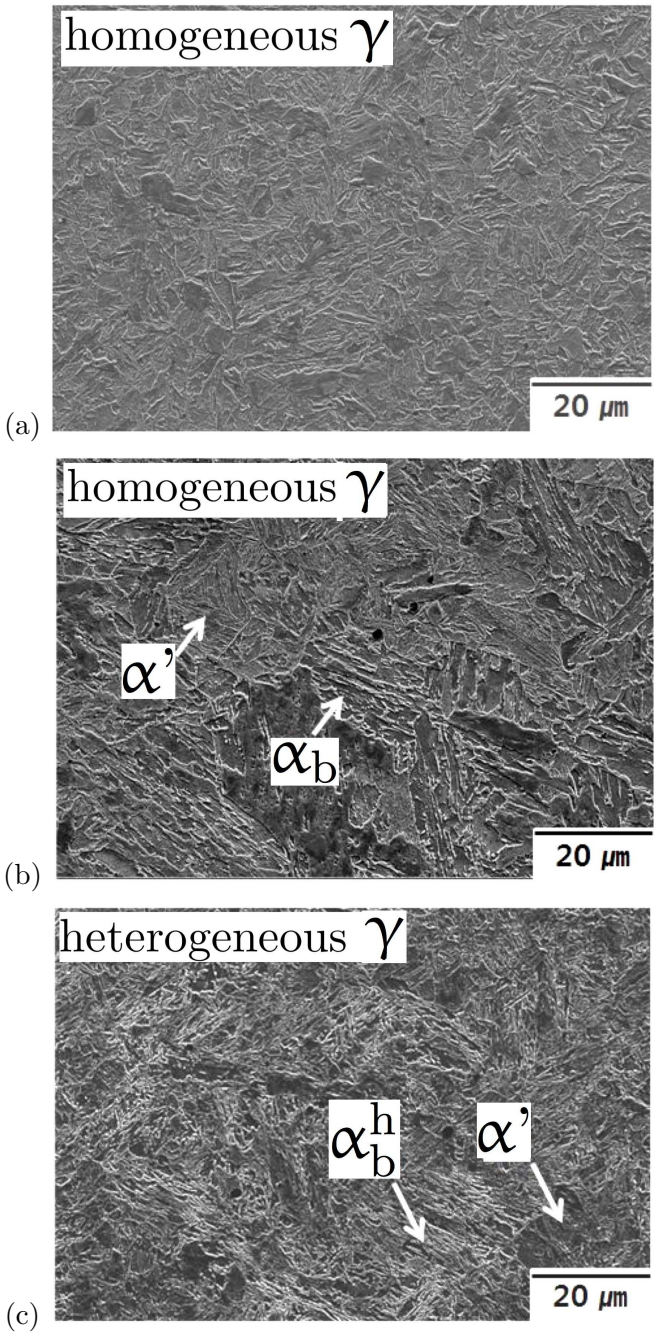

Figure 8: Micrographs showing (a) martensite from homogeneous austenite, (b) mixture of bainite and martensite from homogeneous austenite and (c) similar mixture from heterogeneous austenite.

(a)

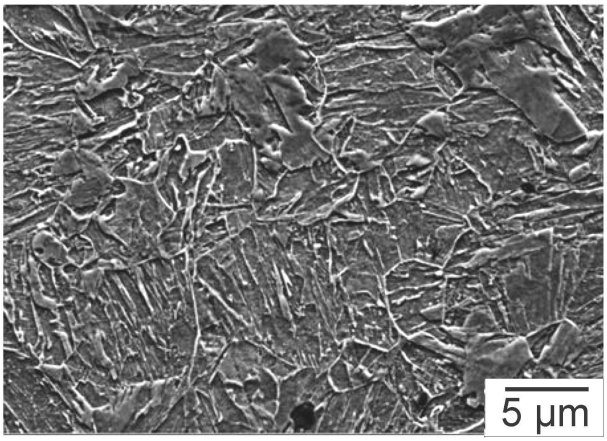

(b)

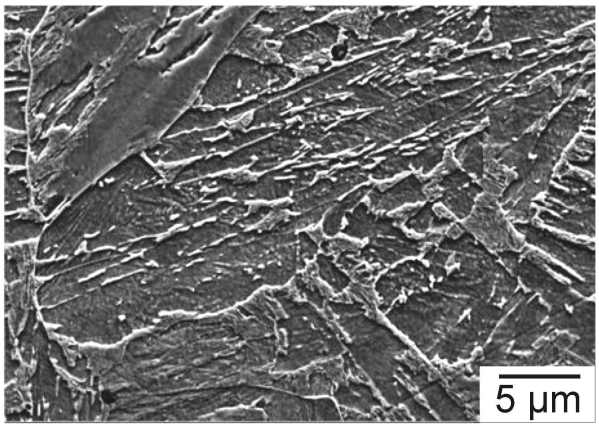

(c)

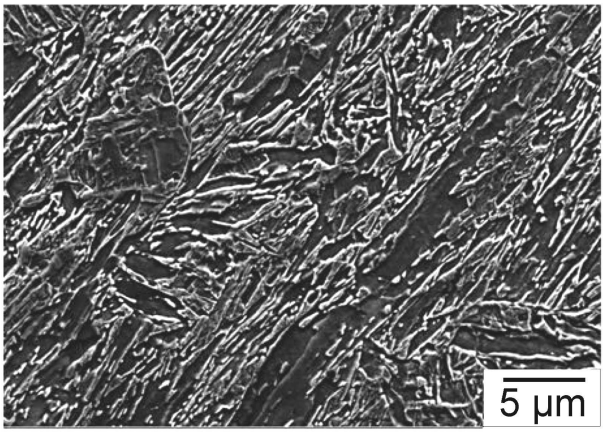

Figure 9: Micrographs showing the detailed structure of (a) martensite from homogeneous austenite, (b) bainite in homogeneous austenite and (c) bainite in heterogeneous austenite.

Figure 10: Transmission electron micrograph of a region extracted using focused ion beam machining from bainite identified using scanning electron microscopy, in the heterogeneous sample. The circled areas were then subjected to microanalysis.

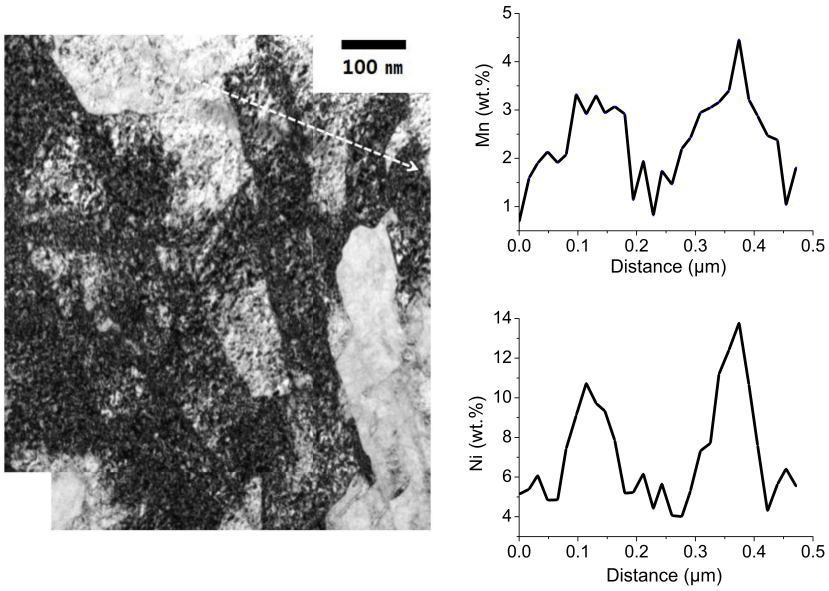

Figure 11: (a) The microstructure including the manganese and nickel–enriched area. The arrow corresponds to the direction of the scan in energy dispersive spectroscopy. (b) The concentration of manganese and nickel along the scan.

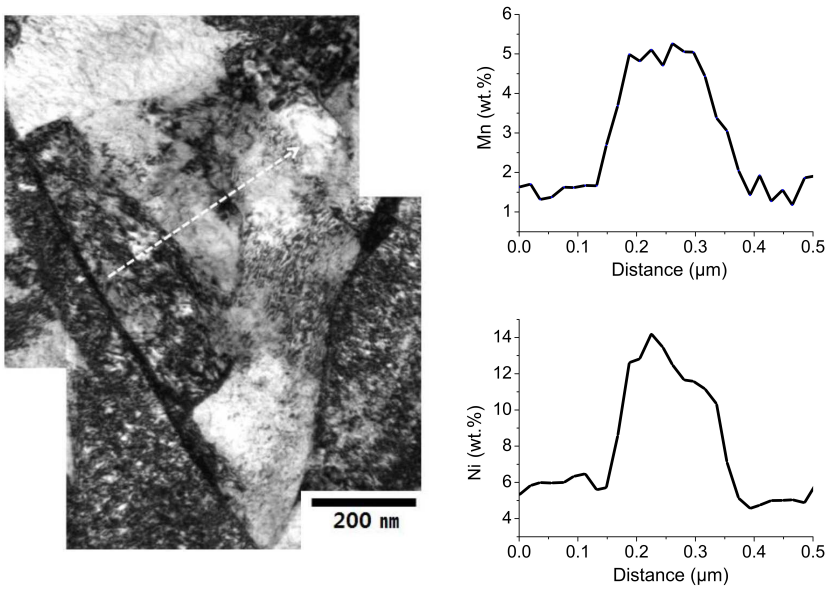

Figure 12: (a) The microstructure including the manganese and nickel–enriched area. The arrow corresponds to the direction of the scan in energy dispersive spectroscopy. (b) The concentration of manganese and nickel along the scan.

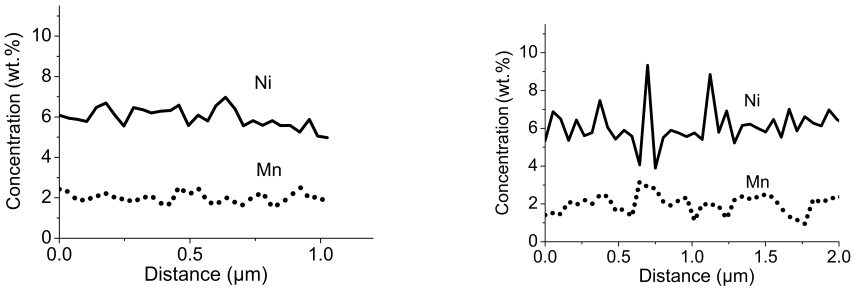

(a) (b)

Figure 13: Additional microanalysis scanning results for manganese and nickel.

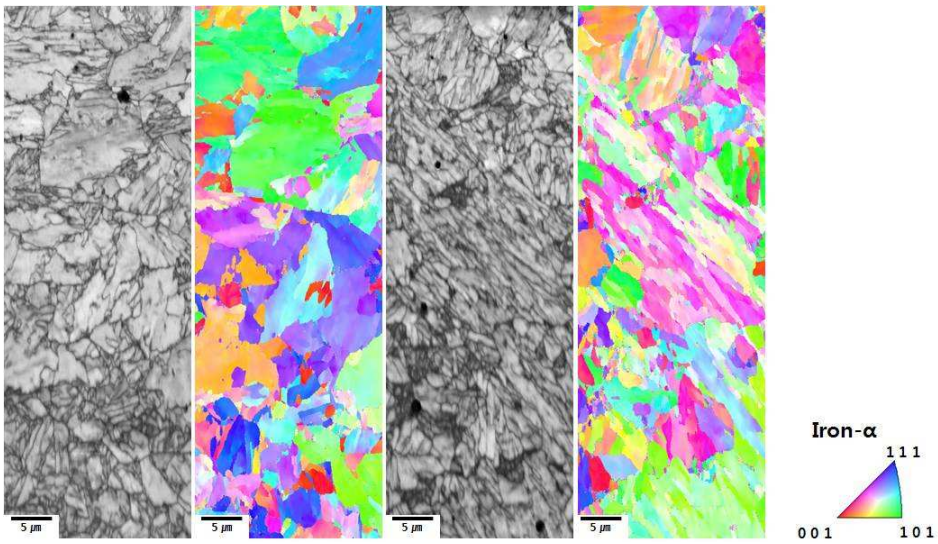

(a) (b) (c) (d)

Figure 14: Image quality and inverse pole figure images of bainite in (a), (b) homogeneous austenite and (c), (d) heterogeneous austenite.